Hindawi
Advances in Civil Engineering
Volume 2022, Article ID 7338718, 11 pages
https://doi.org/10.1155/2022/7338718

Research Article

The Effect of Distance between Sheet Pile and Foundation on Bearing Capacity of Foundation

Aykut Ozpolat and Huseyin Suha Aksoy

Department of Civil Engineering, Firat University, Elazig 23100, Turkey

Correspondence should be addressed to Aykut Ozpolat; aozpolat@firat.edu.tr

Received 3 March 2022; Revised 15 April 2022; Accepted 22 April 2022; Published 6 June 2022

Academic Editor: Zhiguo Zhang

In this study, the presence of a foundation near the sheet pile wall built on sand soil was simulated in the laboratory, similar to the field conditions. For this purpose, laboratory tests of sheet pile wall (SPW) (defo) and bearing capacity (q_{ult}) of the foundation were carried out by applying vertical loads to the steel model foundation. Besides, laboratory tests were represented by the Mohr-Coulomb material model under 3D plane deformation conditions, and numerical analyses were performed. These studies were performed by varying the distance among the SPW, the foundation (L), and the penetration depth of SPW (Hp). The results demonstrated that L had a greater effect on q_{ult} and δmax than the H_p. When L was kept constant and H_p was increased, it was seen that q_{ult} increased and δmax decreased. Moreover, the raise in L has resulted in an increment in the qult and δmax decreased. In addition, a good agreement between numerical analysis and experimental test was observed.

1. Introduction

The increase in urban populations has led to an increase in the need for transportation systems and residential areas. Despite this increase, the useable areas in cities are limited. Therefore, it has become necessary to use existing areas more effectively. New living quarters are often created by deep excavations or by rehabilitating dangerous dip slopes. This has brought stability and safety problems around dangerous dip slopes and deep excavations. During the construction of foundations or deep excavations in urban areas, slope slips and large settlements may occur [1–7]. Lateral support systems are used to prevent dangerous deformations around such construction sites. One of the common lateral support systems is SPWs. SPWs are flexible and generally waterproof structures. They are also used to limit horizontal displacements of the soil mass as lateral support. The reasons SPWs are preferred are that they are economical and save time and space.

Safety and economic efficiency are key objectives in the engineering design [8]. In deep excavations, SPWs are designed according to wall displacement to evaluate their safety and economic efficiency. In this evaluation, two extreme conditions are taken into consideration as follows: one of them is very small deformations, which means that SPW is designed uneconomically; the other one is large displacements, which cause safety problems around the excavation area during construction.

As a result of literature research, some of the studies on excavation stability and safety are as follows: in some papers, numerical studies have been carried out using data from case analyses. In other research studies in the literature are investigated excavation width, wall displacements in the corners of the excavations, support geometry on wall and soil movements, the soil and wall interface, and the effects of wall elasticity are effective onwall-soil deformations. Results from theese studies was mostly compared with case studies [9–14].

In some papers, only numerical analyses were carried out using typical values of soil strength parameters. These studies modeled the construction phase of the diaphragm wall using 3D FEM, generally investigated soil stress distribution mechanisms and soil displacements, stability parameters of 3D rectangular, elastoplastic evaluation of the soil and retaining structure, and wall thickness and wall

penetration depth on retaining walls in their analysis [15–24].

Apart from numerical studies, there are also studies similar to this study. For example, Tan et al. [23] examined the systems for the settlement of buildings adjoining excavations. As a result of their study, it was determined that both the buildings on shallow foundations and those on short piles were sensitive to damage caused by adjoining to deep excavation. This result is different from the popular opinion in the literature.

In the literature, it was seen that the behavior of retaining walls on cohesive soils was examined in general. Numerous studies have been conducted on the behavior that may occur as a result of excavations on retaining walls built on cohesive soils [25–33].

There has been a limited number of literature on the behavior of retaining walls built on sand. These studies were conducted on sand in which an internal friction an angle below 32° was used and the deformations of SPW were investigated [9, 12, 34–36] The effects of the penetration depth and excavation width on the structures around the excavation were examined.

1.1. Research Significance. There are several parameters that affect the bearing capacity of the foundations (q_{ult}) near the retaining structure and the deformations of the retaining structure. These parameters are relative density (D_r), SPW length (H_t), excavation width, the distance between foundation and retaining structure (L), and penetration depth (H_p). It was observed that the effect of only one of these parameters (generally D_r or H_p) on q_{ult} was examined in the literature. The effect of the L parameter on q_{ult} and SPW deformations (δmax) has not been encountered in previous studies. Besides, as can be seen from the literature summary above, some studies were based only on numerical analysis. In some of them, numerical analyses were made using the measurements in the field. This study was based on the effects of L and H_p parameters on q_{ult} and δmax. Except for these two parameters, all other parameters were kept constant.

The soils in the field are generally not homogeneous and consist of different soil layers. The difficulty of determining the soil strength parameters of all layers and the unknown interaction behavior between the layers complicates the stability problems. In such soils, strength parameters related to the soil layers, which are generally accepted strength parameters or obtained from drilling data, are used. This study was based on laboratory experiments and numerical analysis. By simulating a homogeneous soil profile in the laboratory, multilayer effects were prevented and model experiments were carried out. The results obtained were verified by numerical analysis.

2. Material Properties of the Sand and Sheet Pile Wall Used in Model Experiments

2.1. Properties of the Sand. The sand is a dark color river soil and has an angular shape, as shown in Figure 1. Internal friction angles (ϕ) of this material are determined by using a direct shear test, ranging from 42° to 52°, which means the sand has high friction. The material properties of the sand were determined according to ASTM standards [37]; ASTM (D422 - 63 [38]e2, 2007). The granulometry of the soil used in the tests was shown in Figure 2.

Since SPW is driven into the soil with vibration, it cannot be applied on extremely stiff soils. Therefore, in order to provide similarity between field conditions and laboratory model, 16% relative density sand, which is quite loose, was used in the tests. Another objective here was to clearly see the effect of changes in dimensions without changing the properties of the soil. The relative density of the sand was determined according to the ASTM standard [39]. The shear box test on sand was performed according to the ASTM standard [40] and the internal friction angle value was obtained. The material properties obtained are given in Table 1.

The angle of repose of normal loose sand and sand-gravel mixtures is 25–32° [41]. Experiments were carried out to determine the angle of repose of the sand. As a result of this experiment, it was determined that the angle of repose was 35°, as shown in Figure 3. Since the structure of the grains of this sand is angular and basaltic origin, it has a higher internal friction angle than other sands.

2.2. Properties of the SPW. Plexiglass was used as SPW in the tests. The reasons for the use of this material are that its strength and physical properties are standard, and its technical properties are well known. Another reason for using plexiglass as SPW material is that it is easily cut into the desired dimensions, light, and has the capacity to provide the desired deformation in the test. It is known that vinyl material with properties similar to the plexiglass is used in field applications. The material properties of the plexiglass used in the tests can be seen in Table 2.

3. Laboratory Test Procedure and Results

3.1. Test Setup. Due to the stress-dependent soil properties, it is important to accurately model the prototype stress conditions in small-scale modeling experiments. One of the common ways to apply gravity (g)in model experiments is to re-establish the full-size stress levels. Details of the rules and modeling practice used in laboratory modeling can be found in [42]. Information about the scaling laws used in this study is given in Table 3.

Figure 4 and 5 show the plan and cross-sectional view of the modeling test system. İn this study, the in-plane strain condition of the test system is assumed. The conditions and dimensions of the test system are similar in all experiments with the exception of the SPW restraint conditions. Since the experimental system is symmetrical, only half of the system is modeled. While the deep of excavation was 100, 150, 200 mm (The equivalent in the prototype was 10, 15, and 20 m), respectively, the thickness of the sand layer was constant and 950 mm (The equivalent in the prototype was 95 m). The width of the system was 750 mm (The equivalent in the prototype was 75 m). According to the scaling law

Figure 1: Example of flat angular sand particles.

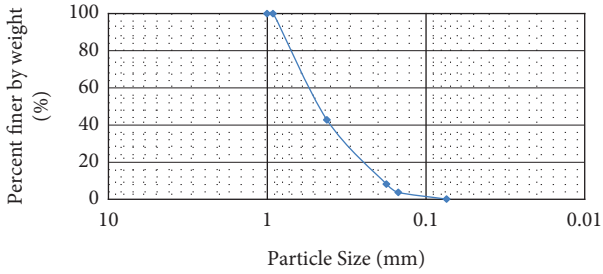

Figure 2: Grain size distribution of the sand.

Table 1: Properties of the material used in the experiment.

Parameters	Values
Specific gravity, G_s (kN/m^3)	2.77
D_{10} (mm)	0.18
D_{30} (mm)	0.32
D_{50} (mm)	0.45
D_{60} (mm)	0.56
C_u	3.11
C_c	1.02
Maximum – Minimum particle size, D_{max}-D_{min} (mm)	1–0.074
Maximum dry density (kN/m^3)	14.3
Minimum dry density (kN/m^3)	17.5
Maximum void ratio, e_{max}	0.903
Minimum void ratio, e_{min}	0.553
Relative density D_r	16%
Soil classification	SP
Angle of internal friction ϕ_{16} (°)	40

given in Table 3, experiment-making procedures were explained and results obtained from the experiments were given. All abbreviations used in the study are given in Table 4.

3.2. Model SPW and Properties. The model SPW was made of 3 mm thick plexiglass sheet and consisted of a single piece. In terms of bending stiffness, the model wall is considered nearly equivalent to a prototype-scale reinforced concrete sheet pile wall. The Young's modulus of these materials, respectively, for plexiglass and concrete is 3.3 GPa and 25 GPa. The ratio of SPW penetration depth to excavation depth is commonly 0.5–2 in engineering application [12, 43, 44]; (100, 150, 200 and 10, 15, 20 m are the model and the prototype dimensions, respectively).

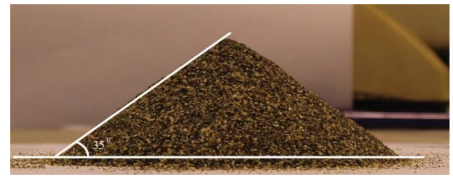

Figure 3: The angle of repose of the sand.

Table 2: Material properties of the plexiglass sheet.

Properties	Values
Density (kN/cm^3)	11.88
Tensile strength (MPa)	70
Flexural strength ((MPa)	90
Elasticity modulus (MPa)	3300

Table 3: Scaling laws.

Physical parameters	Scaling factor (model/prototype)
Gravity (m/s^2)	1
Force (N)	$1/n^3$
Length (m)	$1/n$
Displacement (m)	$1/n^{2-\alpha}$
Area (m^2)	$1/n^2$
Stiffness (N)	$1/n^{\alpha}$
Strain	$1/n^{1-\alpha}$
Density (kg/m^3)	1
Stress (kPa)	$1/n$
α	0.5

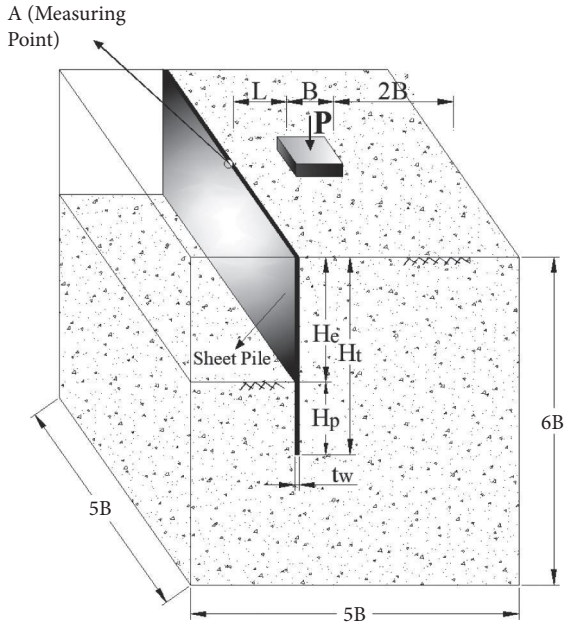

Figure 4: View of the test system.

3.3. Procedure of Model Tests. To investigate the behavior of SPWs on sand, model tests were conducted in the laboratory. The first group of test was performed by keeping H_p constant and changing L. The second test group was carried out by

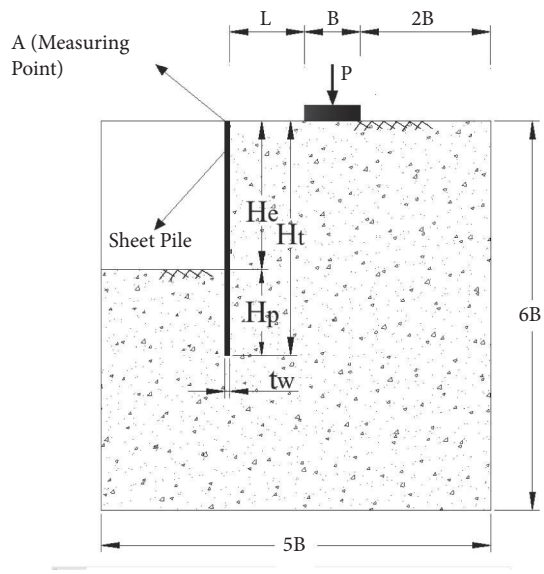

Figure 5: Cross-Sectional view of the test system.

Table 4: Abbreviations.

Symbol	Abbreviation
SPW	Sheet pile wall
q_{ult}	Bearing capacity of foundation
Δmax	Sheet pile wall deformations
D_r	Relative density
H_t	Sheet pile wall length
L	The distance between the SPW and the foundation
H_e	Excavation depth
H_p	Penetration depth of SPW
H_t	SPW total length
t_w	SPW thickness
B	Foundation width
H_x, H_y, H_z	Test tank dimensions
P	Load affecting the model foundation
A	Deformation measurement point

keeping L constant and changing the H_p. As a result of these two groups of tests, δmax and q_{ult} were determined.

The appearance of the model test system are as shown in Figures 4 and 5. According to these figures, H_x, H_y, and H_z are the test tank dimensions, H_t is SPW total length, H_e is excavation depth, H_p is SPW penetration depth, L is distance of the model foundation to SPW, B is foundation width, t_w is SPW thickness, and P is the load affecting the model foundation. The P point in the foundation is where the loads and deformations were measured. Point A is where δmax was measured.

3.4. Scale Effects and Limitations. The loading of the model foundation was carried out with the help of a hydraulic system. Deformation measurements were made at both ends of the foundation and the mid-upper point (point A) of the SPW, as shown in Figures 4 and 5. A $75 \times 75 \times 100$ cm (H_x, H_y, H_z) chamber was used to model the soil environment. A foundation model of $15 \times 15 \times 1$ cm (B) and a plexiglass sheet of $40 \times 75 \times 0.3$ cm (H_t, H_y, t_w) were used during the tests. In model tests, the distance between the test tank wall and the model foundation was designed to be 2B. Similar to the studies performed by Abdelhalim et al. [45]; El Sawwaf and Nazir [46]; Sadrekarimi and Abbasnejad [47], the tank and foundation dimensions were determined by considering that the boundary effects of the tank should be minimal. Thus, in semi-infinite environment conditions, the fundamental rule of model experiments were provided.

The test tank was filled with raining method from a height of 20 cm before placing SPW on the test set. After the filling process was completed, the front part of SPW was excavated until the desired penetration depth was achieved, and loading was started after the model base was placed, as shown in Figure 6 and7. The model foundation was loaded at a speed of about 2.00 mm/min in the tests. The condition of the model foundation and SPW after loading is shown in Figure 8 in order to determine δmax, δmax was taken from point A Figures 4 and 5).

3.5. First Group Test Results. In the experiments, model foundations were loaded with a speed continuous of 1.0 mm/min until a settlement value of 0.1 B consisted. The bearing capacity of the foundation is determined when the deformation reaches 10% of the foundation width, which is 15 mm. The load corresponding to this foundation settlement was determined from the graph, and the bearing capacity of the foundation was determined in this way. This method of determining the q_{ult} has usually been used in model experiments [48, 49]. As a result of the loading tests, the load-settlement graphs for the foundation are obtained in Figure 9.

For $H_p = 20, 25, 30$ cm, the δmax versus L graph is shown in Figure 10. For cases of Hp = 20, 25, 30 cm, SPW had minimum deformations when L was equal to 4 B/3. This δmax was chosen as a reference, and all results were compared with $L = 4$ B/3 to see the effect of L.

In the case of Hp = 20 cm, the decrease of L from 4 B/3 to B, it is caused at δmax an increase of 85.74%. The decrease of L from 4 B/3 to 2 B/3 is caused at δmax an increase of 141.30%. In case of Hp = 25 cm, the decrease of L from 4 B/3 to B is caused at δmax an increase of 84.69%. The decreasing of L from 4 B/3 to 2 B/3 it is caused at δmax by an increase of 124.72%. In case of Hp = 30 cm, the decrease of L from 4 B/3 to B is caused at δmax by an increase of 61.13%. The decrease of L from 4 B/3 to 2 B/3 is caused at δmax by an increase of 97.23%. As seen in the results, δmax decreases with increasing L. When the Hp increases; however, the effect of the change of L on δmax decreases.

As a result of the tests performed, the effect of the foundation load and the change of L value on δmax was measured as in Figure 11, for $H_p = 20$.

As a result of the tests performed, the effect of changing in L on q_{ult} was measured as shown in Figure 12, for Hp = 20, 25, 30 cm. At these 3 penetration depths, in the case of $L = 4$ B/3, the SPW had the minimum deformation and the foundation carried the maximum load. However, when L decreased, δmax increased, and the load carried by the foundation decreased.

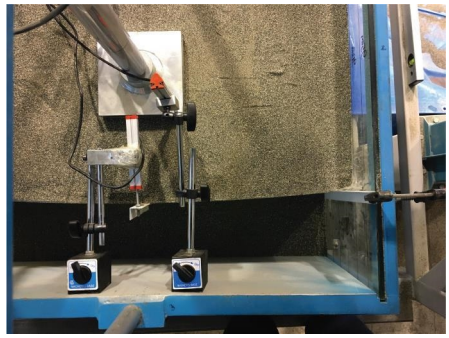

Figure 6: State of SPW before load start – 1.

Figure 7: State of SPW before load start – 2.

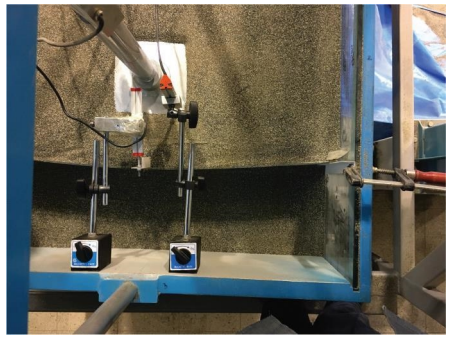

Figure 8: State of SPW after load start.

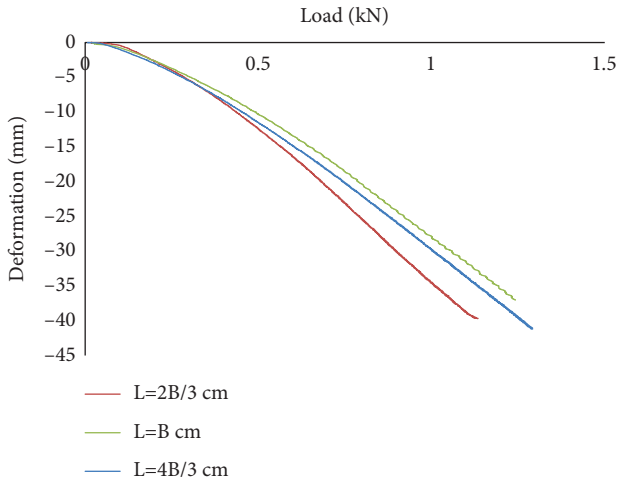

Figure 9: Load vs. foundation settlement in case of $H_p = 25$ cm.

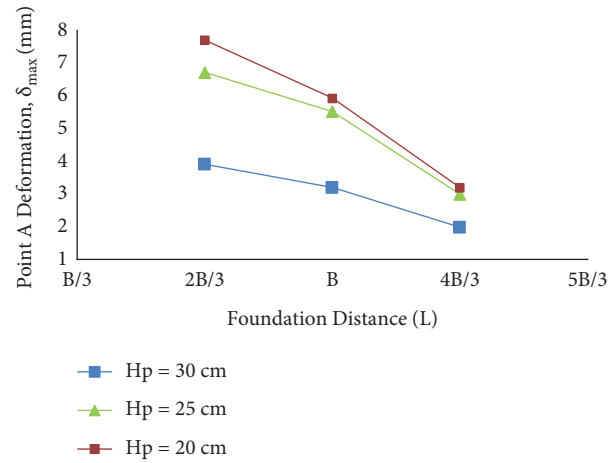

Figure 10: Changes of δmax vs. L in the cases of $H_p = 20, 25, 30$ cm.

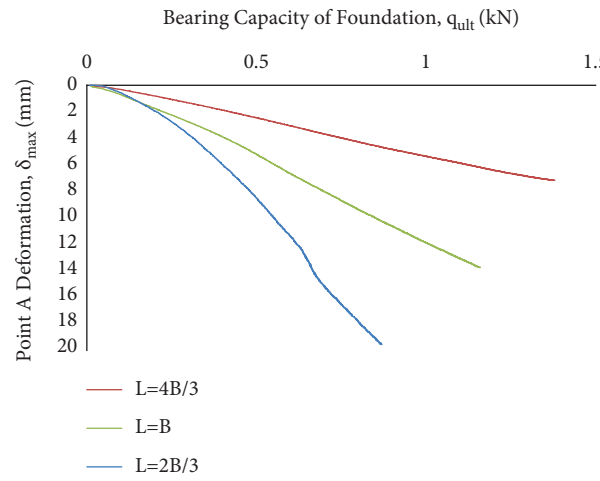

Figure 11: q_{ult} vs. δmax relation in case of Hp = 20 cm.

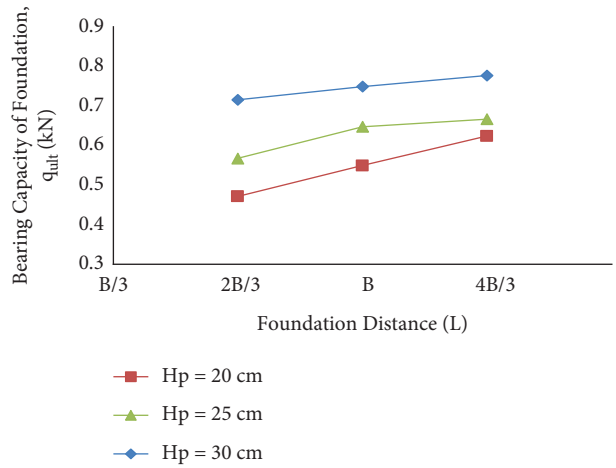

Figure 12: Changes of q_{ult} vs. L in case of $H_p = 20, 25, 30$ cm.

Due to q_{ult} is minimum at $L = 2$ B/3, this q_{ult} value was chosen as a reference, and the other q_{ult} values have been compared with this value to see the effect of L. In the case of

H_p = 20 cm, the decrease of L from 4 B/3 to B is caused at q_{ult} a decrease of 16.55%. The decrease of L from 4 B/3 to 2 B/3 is caused at q_{ult} a decrease of 32.39%. In case of H_p = 25 cm, the decrease of L from 4 B/3 to B is caused at q_{ult} a decrease of 14.04%. The decrease of L from 4 B/3 to 2 B/3 is caused at q_{ult} a decrease of 14.40%. In case of H_p = 30 cm, the decrease of L from 4 B/3 to B is caused at q_{ult} a decrease of 4.69%. The decrease of L from 4 B/3 to 2 B/3 is caused at q_{ult} a decrease of 8.58%. As seen in the results, q_{ult} increases with the increase in L. When H_p increases, the effect of the change in L on q_{ult} decreases.

3.6. Second Group Test Results. For L = 2 B/3, B, 4 B/3, δmax versus Hp are shown in Figure 13. For cases of L = 2 B/3, B, 4 B/3, SPW had minimum deformations when Hp was 30 cm. This δma_x was chosen as a reference and all results were compared with the case of H_p = 30 cm to see the effect of H_p.

In case of L = 4 B/3, the decrease of H_p from 30 cm to 25 cm is caused at δmax an increase of 50.90%. The decrease of Hp from 30 cm to 20 cm is caused at δmax an increase of 61.13%. In case of $L = B$, the decrease of Hp from 30 cm to 25 cm is caused at δmax an increase of 72.97%. The decrease of Hp from 30 cm to 20 cm is caused at δmax an increase of 85.74%. In case of L = 2 B/3, the decrease of Hp from 30 cm to 25 cm is caused at δmax an increase of 71.93%. The decrease of Hp from 30 cm to 20 cm is caused at δmax an increase of 97.13%. As seen in the results, δmax decreases with increasing Hp. When L increases, however, the effect of the change of Hp on δmax decreases.

The effect of load and the change of Hp value on δmax can be seen in Figure 14 for the L = 2 B/3.

As a result of the tests performed, the effect of the change of Hp value on qult was measured as in Figure 15, for Hp values where L = 2 B/3, B, 4 B/3. At these L values, in the case of Hp = 30 cm, the SPW had been the minimum deformation and the foundation carried the maximum load. When Hp decreased, δmax increased, and q_{ult} decreased.

Due to q_{ult} is minimum at H_p = 20 cm, this q_{ult} was chosen as reference and the other q_{ult} values have been compared with this value to see the effect of H_p. In case of L = 2 B/3, the increase of H_p from 20 cm to 25 cm is caused at in q_{ult} an increase of 20.42%. The increase of H_p from 20 cm to 30 cm is caused at in q_{ult} an increase of 51.76%. In case of $L = B$, the increase of H_p from 20 cm to 25 cm is caused at in q_{ult} an increase of 17.82%. The increase of H_p from 20 cm to 30 cm is caused at in q_{ult} an increase of 36.31%. In case of L = 4 B/3, the increase of H_p from 20 cm to 25 cm is caused at in q_{ult} an increase of 6.78%. The increase of H_p from 20 cm to 30 cm is caused at in q_{ult} an increase of 24.47%. As seen in the results, q_{ult} increases with the increase in H_p. However, when L increases, the effect of the change in H_p on q_{ult} decreases.

3.7. Outcome of the Model Tests. The load-deformation data of SPW and the settlement-load data of the foundation were given according to different Hp and L. The effects of different Hp and L on δmax and q_{ult} were analyzed by comparing the data obtained from the first and second group tests. The

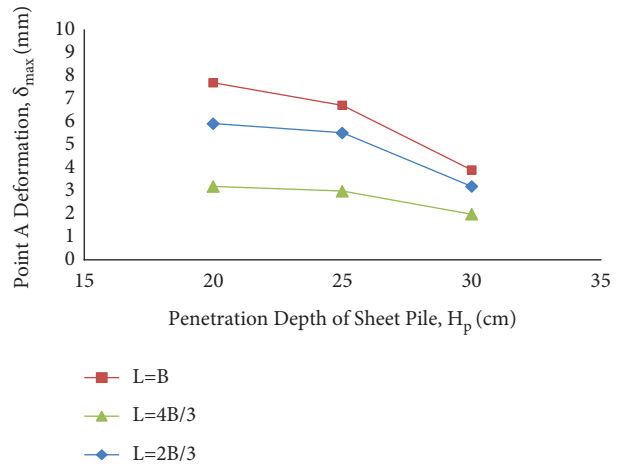

Figure 13: Change of δmax vs. H_p in case of L = 2 B/3, B, 4 B/3.

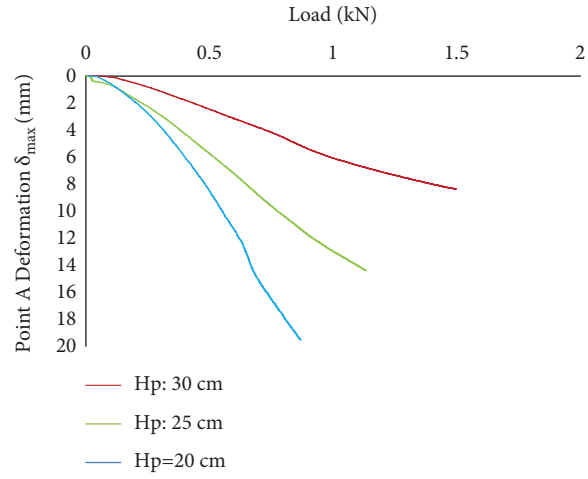

Figure 14: Load vs. δmax relation in the case of L = 2 B/3.

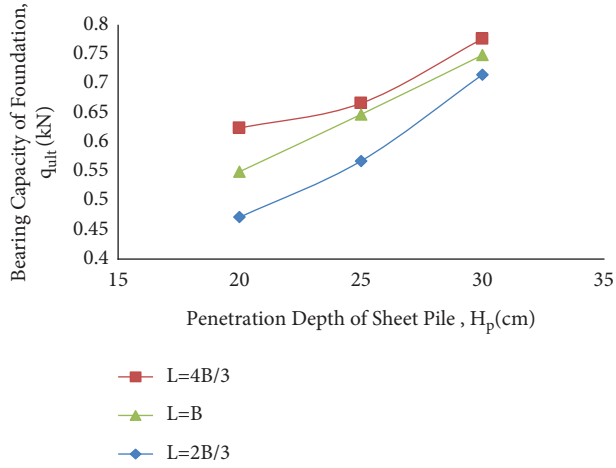

Figure 15: Change of q_{ult} vs. H_p in cases of L = 2 B/3, B, 4 B/3.

δmax corresponding to the maximum q_{ult} obtained in the tests is given in Table 5. The results of q_{ult} are given in Table 6.

Table 5: Maximum δmax obtained from model experiments.

Penetration depth	Sheet pile - foundation distances (L)		
	$L = 2\,B/3$ (mm)	$L = B$ (mm)	$L = 4\,B/3$ (mm)
$H_p = 20$ cm	7.71	5.93	3.19
$H_p = 25$ cm	6.72	5.52	2.99
$H_p = 30$ cm	3.91	3.19	1.98

Table 6: Maximum q_{ult} obtained from model experiments.

Penetration depth	Sheet pile - foundation distances (L)		
	$L = 2\,B/3$ (kN)	$L = B$ (kN)	$L = 4\,B/3$ (kN)
$H_p = 20$ cm	0.472	0.550	0.624
$H_p = 25$ cm	0.567	0.648	0.667
$H_p = 30$ cm	0.716	0.749	0.777

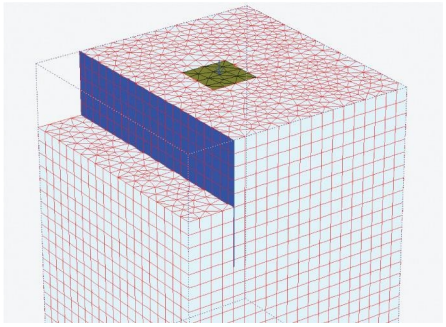

Figure 16: 3D mesh of excavation from the PLAXIS 3D foundation.

Table 7: Plaxis 3D input parameters of sand.

Parameter	Input value for Dr = 16% sand
Cohesion (kN/m^2)	0.001
Unsaturated unit weight (kN/m^3)	14.89
Modulus of elasticity (kN/m^2)	21000
Friction angle (^{0})	40
Poisson's ratio	0.307

4. Numerical Analysis

In numerical study, the effect of H_p and L on the behavior of SPW and q_{ult} was investigated by using FEM. The data obtained were compared to those obtained from the model test. The Plaxis 3D Foundation program was used for numerical simulations performed in this study [50]. In Figure 16, it can be seen that a typical 3D mesh for which a numerical model was created. For 3D analyses, a horizontal midsize mesh and a vertical midsize mesh were used to achieve a balance between the processing time and accuracy.

Similar to the previous studies, the Mohr-Coulomb material model was used in the modeling of the sand [51–59]. In all cases, the cohesion was assumed to be 0.01 kN/m^2. The modulus of elasticity of the soil was taken as $E = 21000$ kN/m^2.

Table 8: Plaxis 3D input parameters of Sheet Pile.

Parameter	Input value
t_w (m)	0.003
Young's modulus (E_1, E_2, E_3) (kN/m^2)	3299000
Poisson's ratio ($\nu 12$, $\nu 13$, ν_{23})	0.35
Shear modulus (G_{12}, G_{13}, G_{23}) (kN/m^2)	1222000

Table 9: Plaxis 3D input parameters of foundation.

Parameter	Input value
Dimensions (cm)	$15 \times 15 \times 1$
Young's modulus (E_1, E_2, E_3) (GPa)	210
Poisson's ratio ($\nu 12$, $\nu 13$, $\nu 23$)	0.3
Shear modulus (G_{12}, G_{13}, G_{23}) (GPa)	79

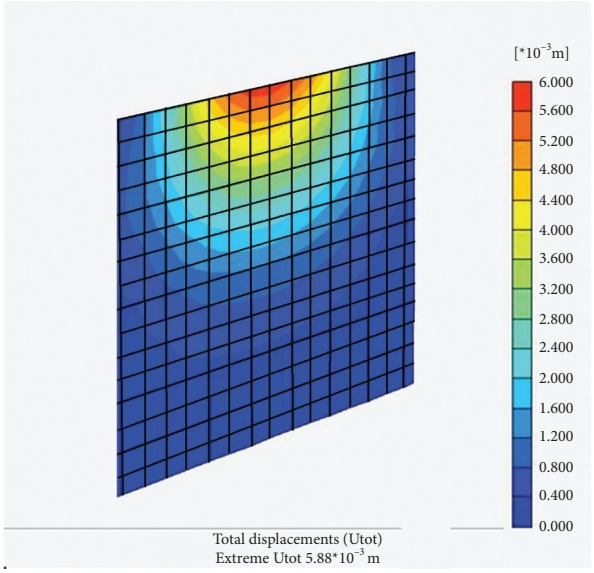

Figure 17: Maximum deformation point of a sheet pile.

In the 3D FEM, the sand was modeled with 10-node tetrahedral elements. 10-node tetrahedral elements provide a second-order interpolation of displacement. The SPW was modeled with 6-node triangular surface element with three translation degrees of freedom per node (U_x, U_y, and U_z). The shear modulus (G) and bulk modulus (K) were obtained using the equations (1) and (2), respectively. The ν in the formulas is the Poisson's ratio.

$$G = \frac{1}{2}\left(\frac{E}{(1+\nu)}\right), \tag{1}$$

$$K = \frac{1}{3}\left(\frac{E}{(1-2\nu)}\right). \tag{2}$$

The properties of sand, SPW, and foundation used in the numerical analysis are shown in Table 7–9, respectively.

In Section1 of the numerical modeling, sand was placed in the soil test tank. Then SPW was driven into sand. The

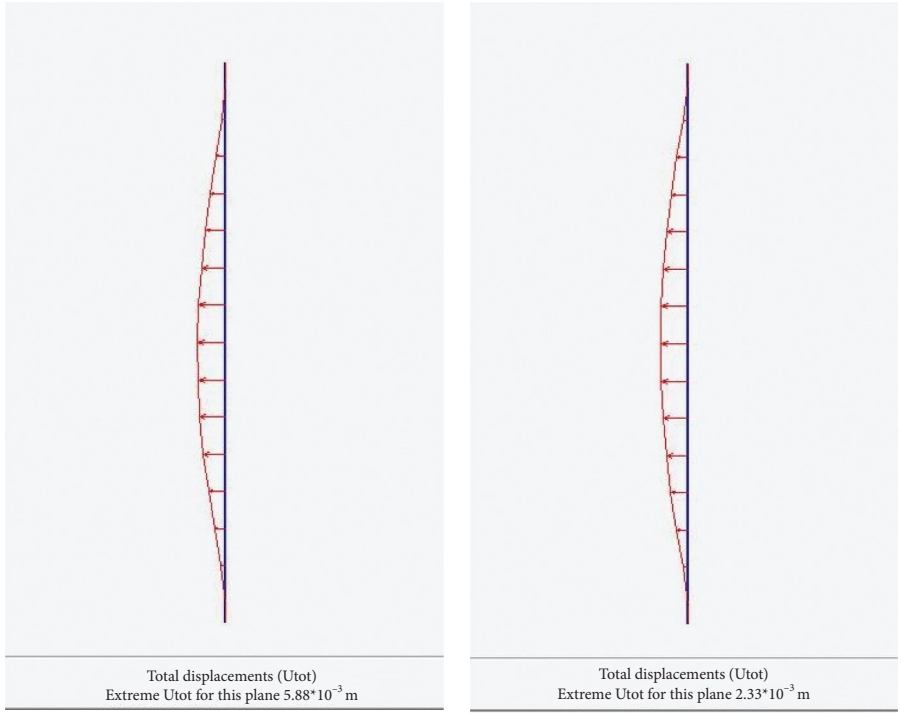

(a) (b)

Figure 18: δmax in case of Hp = 20 cm, $L = B$ cm and Hp = 20 cm, $L = 4$ B/3 cm, respectively.

Table 10: Maximum δmax obtained from numerical analysis.

Penetration depth (H_p)	Foundation (cm) distance (L)		
	$L = 2$ B/3 (mm)	$L = B$ (mm)	$L = 4$ B/3 (mm)
20	7.58	5.88	2.33
25	6.17	5.65	2.76
30	3.90	2.99	1.96

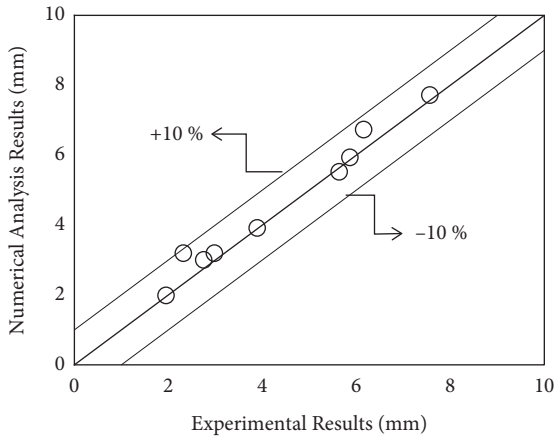

Figure 19: Comparison of data from numerical analyses and laboratory experiments.

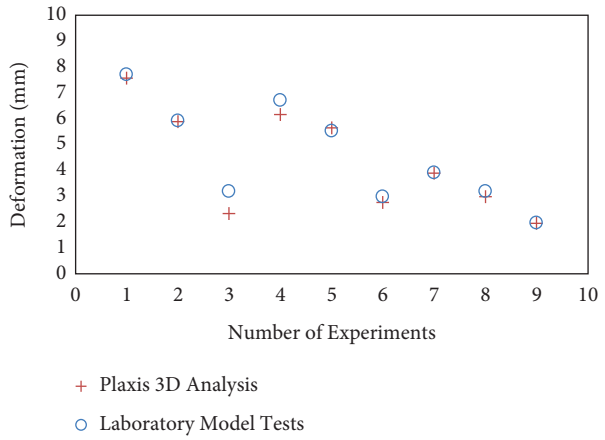

Figure 20: Comparison of data from numerical analyses and laboratory experiments.

excavation was carried out according to H_p in Section 2. In Section 3, the foundation was placed, the load was applied, and the analyses were performed. Finite element models of the wall and foundation were created by using the foundation modeling module and wall modeling modules in Plaxis 3D. After that finite element analyses were made. In the model tests, δmax was taken from point A (mentioned in section 3.1) of SPW. It is clearly seen in Figure 17 that numerical solutions also support this situation.

Numerical analyses were performed by creating the same conditions as the model tests. The maximum load values

obtained from the model tests were applied on the foundation in the numerical analyses and δmax was determined. The δmax obtained as a result of the numerical analyses can be seen in Figures 18(a) and 18(b) and Table 10.

The results obtained from the numerical analyses for δmax values were compared with the results obtained from the model tests, and the comparison can be seen in Figures 19 and 20.

5. Conclusions

In this research, SPW deformations (δmax) and the bearing capacity of the foundations (q_{ult}) close to SPW were investigated by laboratory experiments and numerical analysis.

(i) When penetration depth (Hp) increases, δmax decreases on average by 81% and q_{ult} increases on average by 27%.

(ii) When penetration depth (Hp) decreases, δmax increases on average by 44%, and q_{ult} decreases on average by 38%.

(iii) As the distance between the foundation and the retaining structure (L) increases, δmax decreases by approximately 121% and q_{ult} increases by approximately 16%.

(iv) As the distance (L) between the foundation and the retaining structure decreases, δmax increases by an average of 55%, and q_{ult} decreases by an average of 19%.

(v) Numerical and experimental studies prove that L has great effect on q_{ult} and δmax than Hp. However, both L and Hp do not have much effect on δmax and q_{ult} after a certain distance.

(vi) SPWs should be designed by determining the optimum point for L and Hp values if the field conditions are suitable.

(vii) The results of the Plaxis analyses are more than 90% compatible with the experimental results.

In the present study, the maximum value of L was taken as 4 B/3 due to the geometric conditions of the test system. It is recommended that the effect of L on δmax and q_{ult} can be determined in more detail when different L values are tried in future studies.

Data Availability

The data used to support the findings of this study are included within the article.

Conflicts of Interest

The authors declare that they have no conflicts of interest regarding the publication of this paper.

References

[1] M. Y. Fattah, K. T. Shlash, and H. A. Mohammed, "Experimental study on the behavior of strip footing on sandy soil bounded by a wall," *Arabian Journal of Geosciences*, vol. 8, no. 7, pp. 4779–4790, 2015.

[2] M. Y. Fattah, K. T. Shlash, and H. A. Mohammed, "Bearing capacity of rectangular footing on sandy soil bounded by a wall," *Arabian Journal for Science and Engineering*, vol. 39, no. 11, pp. 7621–7633, 2014a.

[3] Y. Tan and Y. Lu, "Responses of shallowly buried pipelines to adjacent deep excavations in shanghai soft ground," *Journal of Pipeline Systems Engineering and Practice*, vol. 9, no. 2, Article ID 05018002, 2018.

[4] Y. Tan and Y. Lu, "Forensic diagnosis of a leaking accident during excavation," *Journal of Performance of Constructed Facilities*, vol. 31, no. 5, Article ID 04017061, 2017a.

[5] Y. Tan and Y. Lu, "Why excavation of a small air shaft caused excessively large displacements: forensic investigation," *Journal of Performance of Constructed Facilities*, vol. 31, no. 2, Article ID 04016083, 2017b.

[6] Y. Tan and B. Wei, "Performance of an overexcavated metro station and facilities nearby," *Journal of Performance of Constructed Facilities*, vol. 26, no. 3, pp. 241–254, 2012.

[7] Y.-X. Wu, S.-L. Shen, and D.-J. Yuan, "Characteristics of dewatering induced drawdown curve under blocking effect of retaining wall in aquifer," *Journal of Hydrology*, vol. 539, pp. 554–566, 2016.

[8] G. E. Dieter and L. C. Schmidt, *Engineering Design*, 827 pages, McGraw-Hill Higher Education, Boston NY USA, 2009.

[9] S. K. Bose and N. N. Som, "Parametric study of a braced cut by finite element method," *Computers and Geotechnics*, vol. 22, no. 2, pp. 91–107, 1998.

[10] M. Y. Fattah, K. T. Shlash, and H. A. Mohammed, "Experimental study on the behavior of bounded square footing on sandy soil," *Engineering Technology J.* vol. 32, no. 5, pp. 1083–1105, 2014b.

[11] W.-x. Gong, L.-y. Wang, J. Li, and B.-h. Wang, "Displacement calculation method on front wall of covered sheet-pile wharf," *Advances in Civil Engineering*, vol. 2018, pp. 1–13, 2018.

[12] B.-C. B. Hsiung, "A case study on the behaviour of a deep excavation in sand," *Computers and Geotechnics*, vol. 36, no. 4, pp. 665–675, 2009.

[13] Z. Y. Orazalin, A. J. Whittle, and M. B. Olsen, "Three-Dimensional analyses of excavation support system for the stata center basement on the MIT campus," *Journal of Geotechnical and Geoenvironmental Engineering*, vol. 141, no. 7, Article ID 05015001., 2015.

[14] C.-Y. Ou, D.-C. Chiou, and T.-S. Wu, "Three-Dimensional finite element analysis of deep excavations," *Journal of Geotechnical Engineering*, vol. 122, pp. 337–345, 1996.

[15] K. A. K. Al-Juari, M. Y. Fattah, S. I. A. Khattab, and M. K. Al-Shamam, "Experimental and numerical modeling of moving retaining wall in expansive soil," *Geomechanics and Geoengineering*, vol. 16, no. 2, pp. 116–132, 2021.

[16] J. S An, Y. W. Yoon, and K. I. Song, "Feasibility study of an earth-retaining structure using in-situ soil with dual sheet piles," *Geomech. Eng.*vol. 16, no. 3, pp. 321–329, 2018.

[17] Y. Arai, O. Kusakabe, O. Murata, and S. Konishi, "A numerical study on ground displacement and stress during and after the installation of deep circular diaphragm walls and soil excavation," *Computers and Geotechnics*, vol. 35, no. 5, pp. 791–807, 2008.

[18] S. S. Chowdhury, K. Deb, and A. Sengupta, "Estimation of design parameters for braced excavation: numerical study," *International Journal of Geomechanics*, vol. 13, no. 3, pp. 234–247, 2013.

[19] A. T. C. Goh, F. Zhang, W. Zhang, Y. Zhang, and H. Liu, "A simple estimation model for 3D braced excavation wall deflection," *Computers and Geotechnics*, vol. 83, pp. 106–113, 2017.

[20] P.-G. Hsieh, C.-Y. Ou, and Y.-L. Lin, "Three-dimensional numerical analysis of deep excavations with cross walls," *Acta Geotechnica*, vol. 8, no. 1, pp. 33–48, 2013.

[21] S. Jiang, C. Du, and L. Sun, "Numerical analysis of sheet pile wall structure considering soil-structure interaction," *Geomech. Eng.*vol. 16, no. 3, pp. 309–320, 2018.

[22] C. W. W. Ng and R. W. M. Yan, "Three-dimensional modelling of a diaphragm wall construction sequence," *Géotechnique*, vol. 49, no. 6, pp. 825–834, 1999.

[23] Y. Tan, R. Huang, Z. Kang, and W. Bin, "Covered semi-top-down excavation of subway station surrounded by closely spaced buildings in downtown shanghai: building response," *Journal of Performance of Constructed Facilities*, vol. 30, no. 6, Article ID 04016040, 2016.

[24] L. Zdravkovic, D. M. Potts, and H. D. St John, "Modelling of a 3D excavation in finite element analysis," *Géotechnique*, vol. 55, no. 7, pp. 497–513, 2005.

[25] J. Tanner Blackburn and R. J. Finno, "Three-Dimensional responses observed in an internally braced excavation in soft clay," *Journal of Geotechnical and Geoenvironmental Engineering*, vol. 133, no. 11, pp. 1364–1373, 2007.

[26] F. q. Chen, C. Lin, L.-b. Lin, and M. Huang, "Active earth pressure of narrow cohesive backfill on rigid retaining wall of rotation about the bottom," *Soils and Foundations*, vol. 61, no. 1, pp. 95–112, 2021.

[27] G. W. Clough and M. W. Reed, "Measured behavior of braced wall in very soft clay," *Journal of Geotechnical Engineering*, vol. 110, no. 1, pp. 1–19, 1984.

[28] R. J. Finno, J. T. Blackburn, and J. F. Roboski, "Three-Dimensional effects for supported excavations in clay," *Journal of Geotechnical and Geoenvironmental Engineering*, vol. 133, no. 1, pp. 30–36, 2007.

[29] R. J. Finno, D. K. Atmatzidis, and S. B. Perkins, "Observed performance of a deep excavation in clay," *Journal of Geotechnical Engineering*, vol. 115, no. 8, pp. 1045–1064, 1989.

[30] Y. M. Hashash and A. J. Whittle, "Ground movement prediction for deep excavations in soft clay," *Journal of Geotechnical Engineering*, vol. 122, no. 6, pp. 474–486, 1996.

[31] P.-G. Hsieh and C.-Y. Ou, "Shape of Ground Surface Settlement Profiles Caused by Excavation," *Canadian geotechnical journal*, vol. 35, no. 6, pp. 1004–1017, 2011.

[32] G. T. Kung, C. H. Juang, E. C. Hsiao, and Y. M. Hashash, "Simplified model for wall deflection and ground-surface settlement caused by braced excavation in clays," *Journal of Geotechnical and Geoenvironmental Engineering*, vol. 133, no. 6, pp. 731–747, 2007.

[33] G. B. Liu, C. W. Ng, and Z. W. Wang, "Observed performance of a deep multistrutted excavation in shanghai soft clays," *Journal of Geotechnical and Geoenvironmental Engineering*, vol. 131, no. 8, pp. 1004–1013, 2005.

[34] H. S. Aksoy, M. Gor, and E. Inal, "A new design chart for estimating friction angle between soil and pile materials," *Geomechanics and Engineering*, vol. 10, no. 3, pp. 315–324, 2016.

[35] M. Bahrami, M. I. Khodakarami, and A. Haddad, "3D numerical investigation of the effect of wall penetration depth on excavations behavior in sand," *Computers and Geotechnics*, vol. 98, pp. 82–92, 2018.

[36] M. P. Doubrovsky and G. N. Meshcheryakov, "Physical modeling of sheet piles behavior to improve their numerical modeling and design," *Soils and Foundations*, vol. 55, no. 4, pp. 691–702, 2015.

[37] Astm C127-15, *ASTM C127-15: Standard Test Method for Density , Relative Density (Specific Gravity), and Absorption of Coarse Aggregate*, ASTM Standard Book, West Conshohocken PA USA, 2013.

[38] Astm D422-63, *ASTM D422 - 63(2007)e2 Standard Test Method for Particle-Size Analysis of Soils (ASTM 2016)*, ASTM Int West Conshohocken Pa, West Conshohocken PA USA, 2007.

[39] Astm-D698-07, *Standard test methods for laboratory compaction characteristics of soil using standard effort*, ASTM Int West Conshohocken Pa, West Conshohocken PA USA, 2007.

[40] D5321M-17 A D, *ASTM D5321/D5321M-17 (2017),Standard Test Method for Determining the Shear Strength of Soil-Geosynthetic and Geosynthetic-Geosynthetic Interfaces by Direct Shear*, ASTM International, West Conshohocken PA USA, 2017.

[41] J. Liu, G. Wang, T. Kamai, F. Zhang, J. Yang, and B. Shi, "Static liquefaction behavior of saturated fiber-reinforced sand in undrained ring-shear tests," *Geotextiles and Geomembranes*, vol. 29, no. 5, pp. 462–471, 2011.

[42] D. M. Wood, *Geotechnical Modelling (Applied Geotechnics; V. 1)*, p. 504, CRC Press Taylor & Francis Group/Books, Boca Raton FL USA, 2004.

[43] C. W. Ng, J. Wei, H. Poulos, and H. Liu, "Effects of multi-propped excavation on an adjacent floating pile," *Journal of Geotechnical and Geoenvironmental Engineering*, vol. 143, no. 7, Article ID 04017021, 2017.

[44] C. W. W. Ng, Y. Hong, G. B. Liu, and T. Liu, "Ground deformations and soil-structure interaction of a multi-propped excavation in Shanghai soft clays," *Géotechnique*, vol. 62, no. 10, pp. 907–921, 2012.

[45] R. A. Abdelhalim, M. El Sawwaf, A. M. Nasr, and A. Farouk, "Experimental and numerical studies of laterally loaded piles located near oil-contaminated sand slope," *Engineering Science and Technology, an International Journal*, vol. 23, no. 4, pp. 744–757, 2020.

[46] M. El Sawwaf and A. K. Nazir, "Behavior of repeatedly loaded rectangular footings resting on reinforced sand," *Alexandria Engineering Journal*, vol. 49, no. 4, pp. 349–356, 2010.

[47] J. S. Sadrekarimi and A. A. Abbasnejad, "Arching Effect in fine Sand Due to Base Yielding," *Canadian Geotechnical Journal*, vol. 47, no. 3, pp. 366–374, 2010.

[48] A. B. Cerato and A. J. Lutenegger, "Bearing capacity of square and circular footings on a finite layer of granular soil underlain by a rigid base," *Journal of Geotechnical and Geoenvironmental Engineering*, vol. 132, no. 11, pp. 1496–1501, 2006.

[49] A. J. Lutenegger and M. T. Adams, "Bearing capacity of footings on compacted sand," in *Proceedings of the 4th Int. Conf. Case Hist. Geotech. Eng*, Missouri, USA, June 1998.

[50] R. B. J. Brinkgreve, W. M. Swolfs, E. Engin et al., "PLAXIS 2D 2010. User Manual," *Plaxis Bv*, vol. 13, pp. 978–990, 2010.

[51] Ö. Bilgin and M. B. Erten, "Analysis of Anchored Sheet Pile Wall Deformations," *American Society of Civil Engineers*, pp. 137–144, 2009.

[52] R. A. Day and D. M. Potts, "Modelling sheet pile retaining walls," *Computers and Geotechnics*, vol. 15, no. 3, pp. 125–143, 1993.

[53] C.-C. Fan and J.-H. Luo, "Numerical study on the optimum layout of soil-nailed slopes," *Computers and Geotechnics*, vol. 35, no. 4, pp. 585–599, 2008.

[54] L. Grande, O. K. Soreide, and T. H. Tefera, "Large scale model testing on the moment distribution and deformation behaviour of a sheet pile wall," in *Proceedings of the 2nd International Conference on Soil Structure Interaction in Urban Civil Engineering*, pp. 389–394, Zurich, Switzerland, 2002.

[55] H. P. Neher and A. Lachler, "Numerical modeling of a diaphragm wall production process in Rotterdam compared to monitoring data," in *Proceedings of the Sixth European Conference on Numerical Methods in Geotechnical Engineering*, pp. 417–422, Graz Austria, 2006.

[56] D. M. Potts and A. B. Fourie, "The Effect of wall Stiffness on the Behaviour of a Propped Retaining wall," *Geotechnique*, vol. 35, no. 3, pp. 347–352, 2015.

[57] D. M. Potts and A. B. Fourie, "The Behaviour of a Propped Retaining wall: Results of a Numerical experiment," *Géotechnique*, vol. 36, no. 1, pp. 119–121, 1986.

[58] Y. Tan and Y. Lu, "Parametric studies of DDC-induced deflections of sheet pile walls in soft soils," *Computers and Geotechnics*, vol. 36, no. 5, pp. 902–910, 2009.

[59] Y. Tan and S. G. Paikowsky, "Performance of sheet pile wall in peat," *Journal of Geotechnical and Geoenvironmental Engineering*, vol. 134, no. 4, pp. 445–458, 2008.